Chapter

Perovskite-Based Materials for Energy Applications

Mirela Dragan, Stanica Enache, Mihai Varlam and Konstantin Petrov

Abstract

The role of energy in modern society is fundamental. Constraints due to the emissions of air pollutants from the excessive use of fossil fuels have increased dramatically in the last years. Over the years various devices and systems have been developed to transform energy from forms supplied by nature to forms that can be used by people. Another issue is to absorb energy generated at one time and to discharge it to supply power at a later time, what is called energy storage. This is also a matter to focus when it comes to searching for solutions of energy problems. Perovskites are promising key materials for energy applications, and in this chapter is a literature review summarizing the reported progress in energy applications of perovskite-type ceramic materials. To understand the fundamental nature of structure–property relationships, defect chemistry plays an important role. This paper, a mini-review, briefly describes from available literature and summarizes accordingly. It is focused on perovskite crystal structures, perovskite materials for solid oxide fuel cells, perovskite electrocatalyst and photocatalysts, and perovskite transport features.

Keywords: perovskite, perovskite crystal structure, defect chemistry, perovskite synthesis, transport properties

1. Introduction

There is going to be huge demand for energy. The growing population and the growing of industrialization will increase the demand for energy. The world needs *more energy* to allow global living standards to continue to improve.

Currently most of our energy comes from fossil fuels, which originated from deep within the Earth's crust. This had disastrous effects on the planet because the burning of coal, oil, and gas has been linked to the rising levels of greenhouse gases on the Earth's atmosphere, generating climate change. The global energy landscape requires improvements. There is a slow going on transition to a more sustainable energy system. Not only to meet the need of rising energy demand but also in terms of policy, reducing carbon emission energy systems is the biggest challenges of our time.

Along with these challenges come opportunities—and that is what makes this a really exciting time for material science with respect to efficient and cost-effective energy conversion and energy storage. The process of changing energy from one

form to another is energy conversion, and energy storage is the capture of energy produced at one time for use at a later time.

This work aims to provide an overview, based on available literature, of perovskite materials for energy applications and will focus especially on solid oxide fuel cells for efficient power generation from fuels and electrocatalysts for oxygen reduction reaction, oxygen evolution reaction, as well as on the defect chemistry in general of such materials. A large number of articles related on this topic have been published in the past decades. Unfortunately, it is not possible to cover all the aspects and references in the literature.

Due to their properties, the perovskite materials are of considerable technological importance covering a very broad range of practical applications. Notable is the discovery in the 1940s of the ferroelectric properties of barium titanate ($BaTiO_3$) used in electronics for capacitors and transducers [1]. In the mid-1980s, the first high-temperature superconductor was discovered, lanthanum barium copper oxide and, in 1987 Nobel Prize in physics, was awarded for this discovery [2]. As of 2012, perovskites have been identified as possible inexpensive base materials for high-efficiency commercial photovoltaics, and perovskites also have optoelectronic properties such as strong light absorption and facilitated charge transport [3]. Some of perovskites' typical properties are ferromagnetism [4], piezoelectricity [5, 6], electrical conductivity [7, 8], superconductivity [9, 10], ion conductivity [11, 12], magnetism [13, 14], catalytic properties [15, 16], electrode materials [17, 18], and optical [19, 20].

This work will describe their defect chemistry which plays an important role in energy applications where the transport properties are the main players. Their defect chemistry is responsible for properties like ionic conductivity [21], mixed conductivity [22], proton conductivity [23], and catalytic conductivity [24] which make perovskite being used for solid oxide fuel cells (SOFC), electrolyte, SOFC electrode, and catalyst.

2. Perovskites and related structures

The perovskite structure is adopted by many compounds residing on the generic formula ABX_3, the same type of crystal structure as calcium titanium oxide ($CaTiO_3$), constituting the family of perovskite compounds. We owe the discovery of perovskite to Gustav Rose, a German mineralogist who performed the studies in

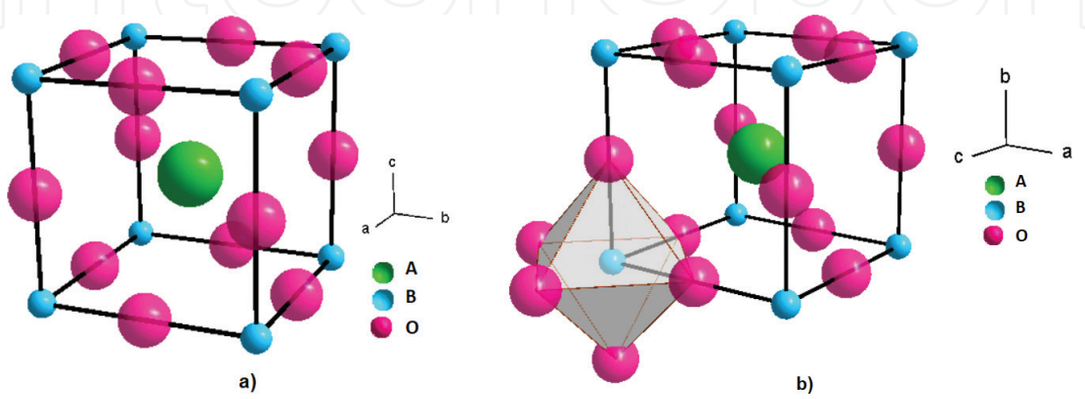

Figure 1.
Cubic perovskite unit cell. Green spheres represent A cations, blue spheres represent B cations, and red spheres represent oxygen anions forming an octahedron. (a). In the perovskite structure with the large cation at the cube center, the small cations are on the corners, and the anions are located at the midpoint of each edge. (b). It emphasizes the octahedral coordination of the small cation.

the Ural Mountains in Russia back in 1893. During that time, he identified perovskite, a naturally occurring oxide species, with the chemical formula $CaTiO_3$ and named it after Russian mineralogist Count Lev Alekseyevich von Perovski [25].

The ideal perovskite-type structure is cubic with space group Pm3m [26]. The positive charge B-type cations are occupying the centers of corner-shared octahedra of negative charge X-type anions such as oxygen halides, sulfides, or nitrides, and positive charge A-type cations are filling the resulting interstices. We restrict this

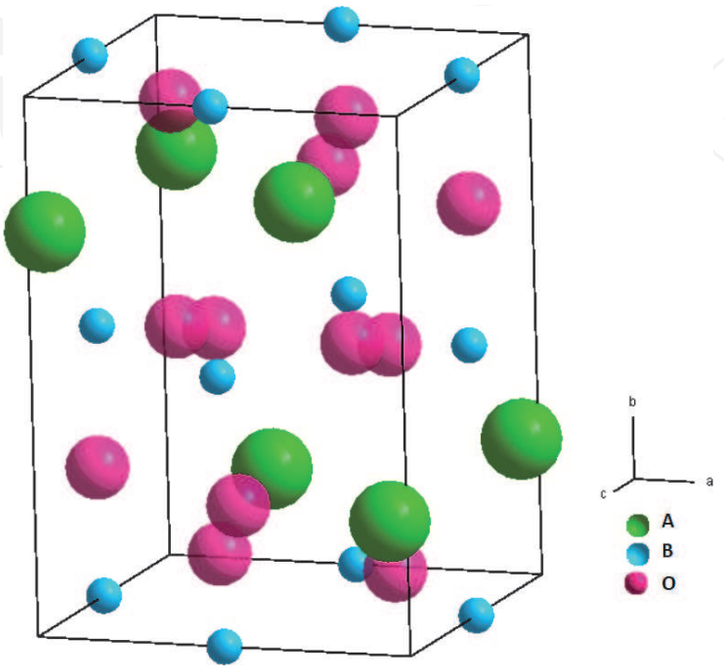

Figure 2.
The orthorhombic phase of perovskite. Green spheres represent A cations, blue spheres represent B cations, and red spheres represent oxygen anions.

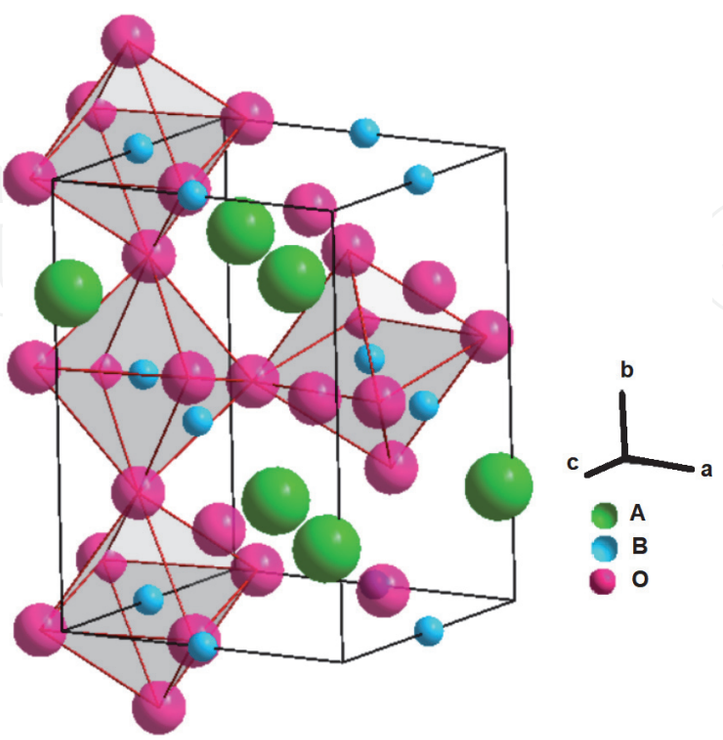

Figure 3.
The tetragonal phase of perovskite. Green spheres represent A cations, blue spheres represent B cations, and red spheres represent oxygen anions.

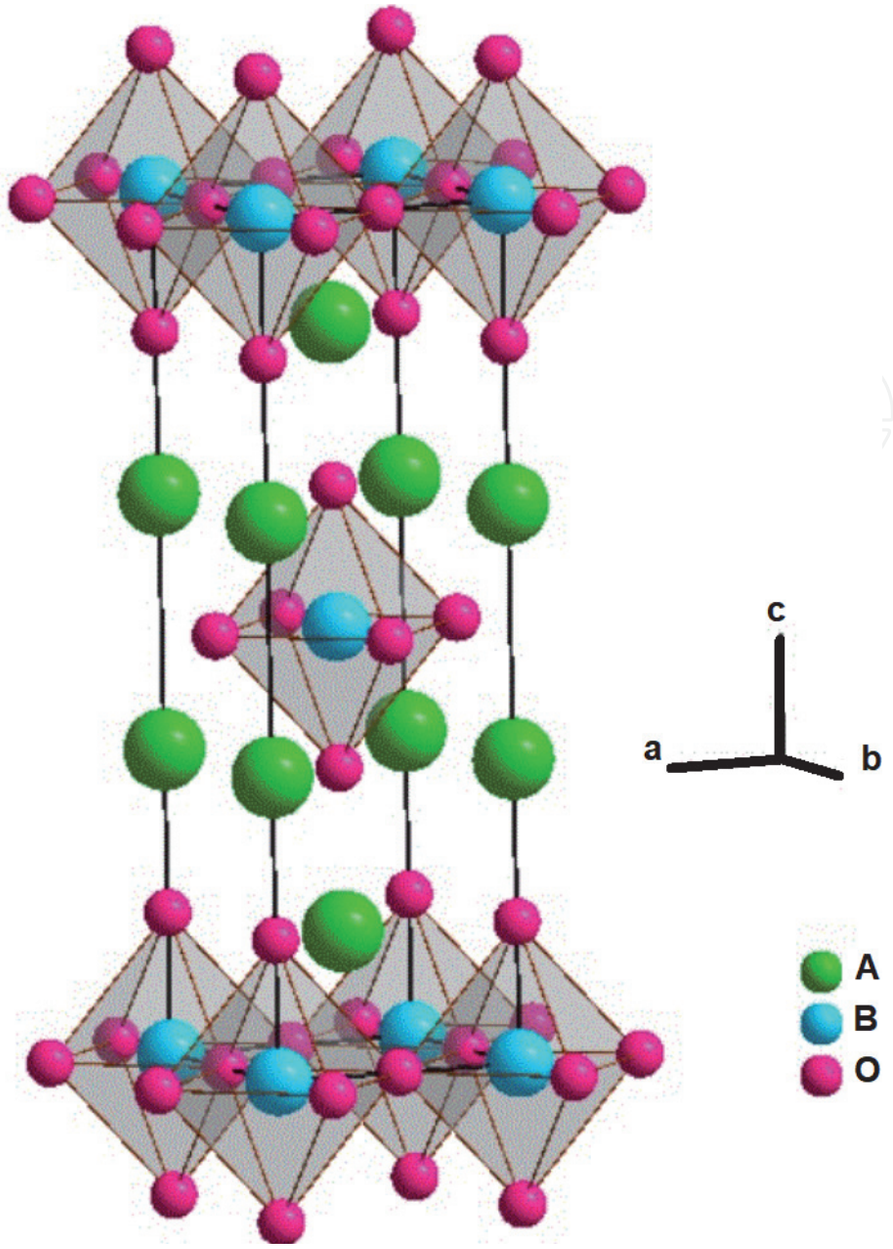

Figure 4.
The Ruddlesden-Popper phases. Green spheres represent A cations, blue spheres represent B cations, and red spheres represent oxygen anions.

study to the oxide perovskites. In **Figure 1a**, alternative ways to view the perovskite structure are displayed: the cubic perovskite unit cell. **Figure 1b** emphasizes the octahedral coordination of the small cation. Green spheres represent A cations, blue spheres represent B cations, and red spheres represent oxygen anions forming an octahedron. Most perovskites are distorted and do not have the ideal undistorted cubic structure. Few perovskite compounds actually form the ideal cubic structure. The mineral perovskite itself, calcium titanate $CaTiO_3$, is an orthorhombic distortion of the basic structure; strontium titanate $SrTiO_3$ is often used as the prototype.

The equation determined by Goldschmidt correlates geometrically crystal structures in terms of the ionic packing using the Goldschmidt's tolerance factor *t* [27]. Favorable for cubic perovskite structure is the tolerance factor having values between 0.8 and 1; otherwise the ideal cubic structure is a distorted structure. Empirical mathematical expression involving the unit cell length ratio, here r_A, r_B, and r_O, is the ionic radii for A, B, and O, respectively; t is given as

$$t = \frac{(r_A + r_O)}{\sqrt{2}(r_B + r_O)} \quad (1)$$

Cations with large ionic radius are occupying A sites, and cations with smaller ionic radius are occupying B sites. A and O form cubic closest packing, and B is in the octahedral voids in the packing. In an ideal structure, where the atoms are

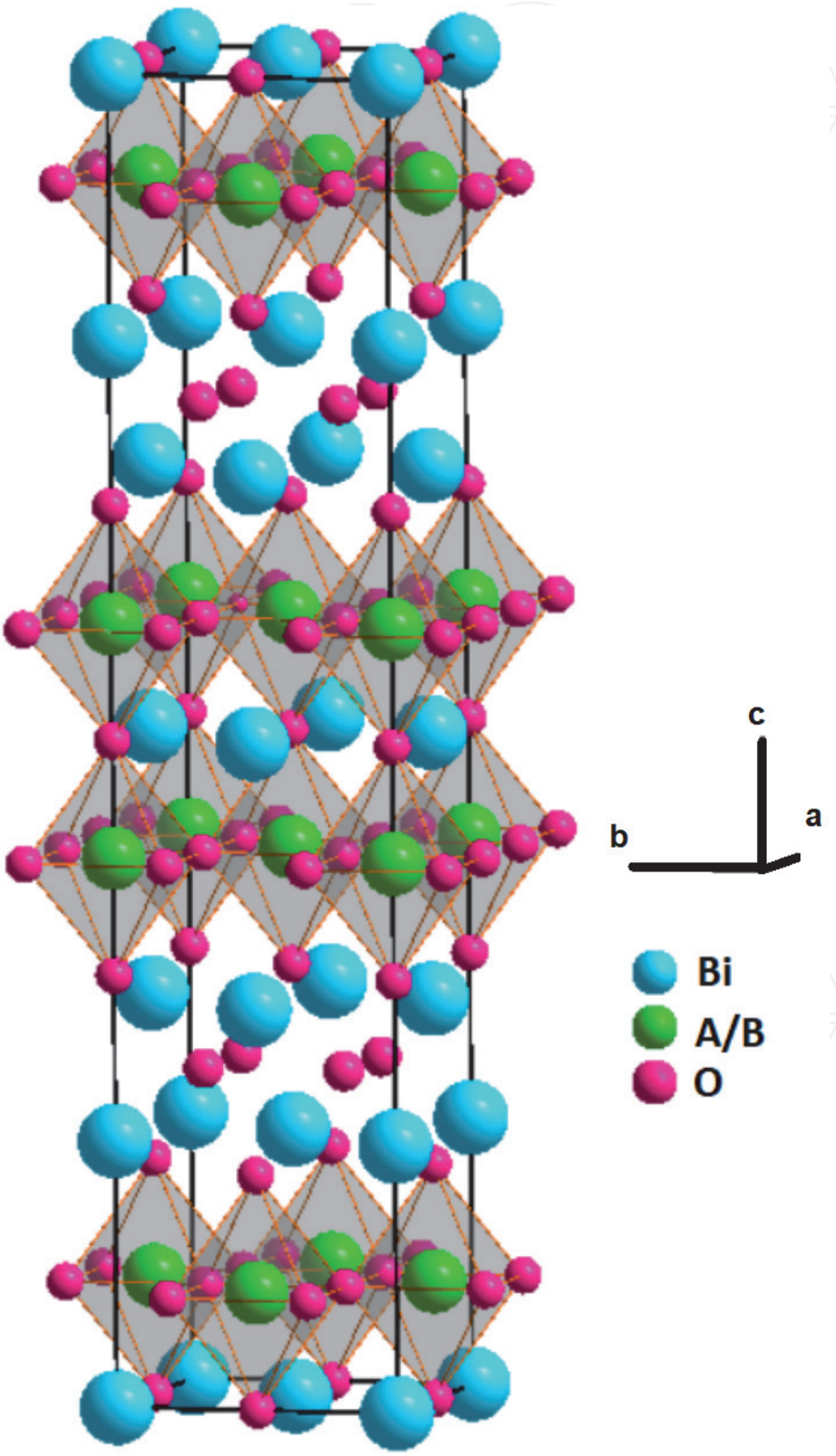

Figure 5.
The Aurivillius n = 1 structure. Green spheres represent A cations, blue spheres represent B cations, and red spheres represent oxygen anions.

simply bonding to one another, the B-O distance is equal to a/2, whereas the A-O distance is equal to $(a/\sqrt{2})$ where a = length of unit cell.

The orthorhombic (**Figure 2**) and tetragonal (**Figure 3**) phases are the most common non-cubic variants [26] with octahedral distortions and translational A site offsets. As previously mentioned, green spheres represent A cations, blue spheres represent B cations, and red spheres represent oxygen anions.

Perovskites allow chemical tailoring because of the wide range of ions and valences which they can accommodate. By suitable formulation many valuable properties can be tailored. One interesting quality of perovskites is that they can accommodate more than one element for both A- and B sites constituting complex perovskites. These can be represented as $(A^1_{1-x}A^2_x)BO_3$, $A(B^1_{1-x}B^2_x)O_3$. Substitutional aliovalent cations residing on the host cation sites generate oxygen vacancies. Furthermore for the B site, the element of transition metal can be in different oxidation states $A(B'_xB''_y)O_3$, where x + y = 1. Aliovalent substitutions require a charge compensation mechanism because the ionic compound must be neutral. Therefore, either ion vacancies are created or one of the metals is partially or fully reduced or oxidized.

Another interesting and useful to deal with is the complex set of phase relationships. These are useful in such materials because they are sensitive to external conditions, including temperature, pressure, strain, and composition [28].

The perovskite structure also lends itself to the building of superstructures as seen in **Figure 4**. The Ruddlesden-Popper phases are a series of structures consisting of sequences of max 3 n; perovskite blocks are separated by a rock-salt structure block. The first member of the Ruddlesden-Popper series is A_2BO_4 or ABO_3-AO which is isostructural with potassium tetrafluoridenickelate (II) K_2NiF_4, the prototype structure.

A second family of superstructures are the Aurivillius phases (**Figure 5**) [29]. This is represented by the general formula $(Bi_2O_2)(A_{n-1}B_nO_{3n+1})$, where A is a large monovalent, divalent, or trivalent 12-coordinate cation and B is a small trivalent, pentavalent, or hexavalent metallic 6-coordinate cation. Basically, their structure is built by alternating layers of $[Bi_2O_2]_2^+$ and perovskite blocks $(A_{n-1}B_nO3_{n+1})_2$ that contain a layer of octahedral B sites.

Various synthesis methods have been developed for the preparation of perovskite materials while managing efficiently the environmentally friendly processing in conjunction with phase structure tailored to the needed properties. Small changes in the crystal will have a large impact on functional properties, crystallinity, and stability. Among these techniques, dry ways like solid-state reaction mechanochemical processing or wet routes like sol–gel and microwave methods are widely used.

3. Perovskite defect chemistry

In crystalline state an array of atoms is regularly repeated in three dimensions. This construction leads to a perfect crystalline solid with all atoms present and located in their ideal positions. However, a zero entropy is needed for the perfect crystalline state to exist. Above absolute zero temperature is a probability that defects from ideality will exist. All real materials contain defects. These defects, in terms of dimensionality, can be vacancies and interstitials which are point defects, dislocations which are line defects, and grain boundaries which are plane defects.

Point defects cause an increase of the configurational entropy contribution to the free energy at nonzero temperatures and will therefore always be present.

The formation of a point defect can be considered as a chemical reaction. At constant temperature, T, and pressure, p, the reaction is carried on in the direction that lowers the Gibbs free energy as follows:

$$G = U + pV - TS = H - TS \tag{2}$$

where H is the enthalpy, U is the internal energy, S is the entropy, and V is the volume. The enthalpy H is defined as

$$H = U + pV \tag{3}$$

The change in free energy for the formation of n independent defects can be written as follows:

$$\Delta G = n\Delta_f G - T\Delta_f S_c \tag{4}$$

In the above equation, the configurational entropy $\Delta_f S_c$ is the part of the entropy change associated with randomly distributing n defect in the material. For a single defect, the formation free energy $\Delta_f G$ is independent of the number of defects and can be written as follows:

$$\Delta_f G = \Delta_f U + p\Delta_f V - T\Delta_f S \tag{5}$$

The point defects are a nonstoichiometric perturbation of the ideal lattice having or not electrically charge. Materials can also be prepared in such a way as to increase the number of defects.

There are two main categories for point defects: intrinsic defects and extrinsic defects. The intrinsic defects are internal to the crystal. The extrinsic defects are created when an impurity atom or ion is inserted into the lattice. The main categories of intrinsic defects are Schottky disorder and Frenkel disorder.

The Schottky disordering mechanism presumes that atoms leave their sites in the crystal bulk and rebuild the crystal lattice on the surface. As a result, the vacancies are formed in both cation and anion sublattices. According to the Frenkel mechanism, an atom moves from its regular site to the nearest interstitial position; hence, two types of defect are formed in the crystal, namely, the vacancy and the interstitial atom.

A vacancy is formed if an atom is not present on the site that it should occupy in a perfect crystal. By removing one atom from the chemical formula of perovskite, a set of vacancies called Schottky defect is created, which is the removal of an oxygen atom. Oxygen ion has a charged of −2. The defect left behind after removal, a charge of +2, for an oxygen atom will be $V_{\ddot{O}}$ in Kröger-Vink notation. The following equation is written for the creation of oxygen vacancy, Schottky disorder:

$$O_O^X = \frac{1}{2}O_2 + V_{\ddot{O}} + 2e' \tag{6}$$

V indicates a vacancy, the subscript O indicates the oxygen host site, and superscript denoted by two dots is the defect charge of +2.

An interstitial is an ion situated on any site that would be unoccupied in a perfect crystal. The interstitial is denoted by a subscript *i*, in Kröger-Vink notation. Frenkel defects deal with the displacement of the ions from its sites to interstitial sites.

When an ion is substituted with an ion of different valence, another type of point defect is created, called substitutional defect.

Defect chemistry complies with the conservation rules which indicate the charge conservation by maintaining crystal electrical neutrality overall, and the mass balance and host structure should be preserved.

The possible point defects in ABO_3 perovskite are the oxygen vacancies, A site vacancies, B vacancies, A interstitials, and B interstitials. The metal interstitial, B interstitial, defects are not energetically favored and less likely to be present.

Let us have a look at the $LaCoO_3$ simultaneous doping on the A site and B site, with Sr., respectively, Fe and Cr. This is a way to increase oxide ion conductivity and at the same time to retain the required thermodynamic stability of doped lanthanum cobaltite.

Substitution of Cr^{3+} for Co^{3+} in the $LaCoO_3$ results in the formation of Cr^{4+} according to the reaction

$$Co_{Co}^{X} + Cr_{Co}^{X} = +Co'_{Co} + Cr_{Co}^{\bullet} \tag{7}$$

The charge disproportionation equation for Co site is

$$2Co_{Co}^{X} = Co_{Co}^{\bullet} + Co'_{Co} \tag{8}$$

Using Kröger-Vink notations Co_{Co}^{X}, $Co_{Co}^{\bullet}$, Cr^{4+}, Co'_{Co}, Cr_{Co}^{X}, and $Cr_{Co}^{\bullet}$ indicates Cr^{3+}, Co^{4+}, Co^{2+}, and Cr^{3+}, respectively.

For the ions of Fe^{3+} doping on the Co^{3+} site, is a similar behavior. Their interaction is leading to form Fe^{2+}, Fe^{4+} and Co^{2+}, Co^{4+}, respectively.

Sr^{2+} on La^{3+} sites is represented by the negatively effective charged Sr'_{La}.

Within the framework of standard band approach, thermally activated electrons can jump from the valence band via the bandgap toward the conduction band. For conduction band electrons e and valence band holes h, the relevant equation is

$$nil = e' + h^{\bullet} \tag{9}$$

A free electron in the conduction band and an itinerant hole in the valence band appear simultaneously.

Owing to its intrinsic zero-dimensional nature, a point defect, or any single atom, is difficult to observe experimentally, and much of the knowledge about point defects is inferred by implicit methods.

4. Perovskites transport properties

The key important factors for the ionic transport of perovskite materials are their defect chemistry and crystal structure. Point defects, mainly ionic defects, have major impact on transport properties like ionic diffusion and ionic conductivity. These properties are the most important in technical applications mentioned in this chapter, dealing with movement of ions within crystal.

Vacancies, interstitials, and substitutional defects can all be charged. The linear response that relates the current density to the applied field is the conductivity. This proportionality constant can be expressed as follows:

$$I_i = \sigma_i E \tag{10}$$

where E is the applied electric field in V^*cm^{-1}, I_i is the current density for species i in A^*cm^{-2}, and σ_i is the conductivity σ_i in $1^*\Omega^{-1*}cm^{-1}$.

The charge may be transported by electrons or holes, by ions, or by both. There are also solids that exhibit simultaneously significant levels of both ionic and electronic transport and are referred to as mixed conductors, MIECs. While ionic conduction is mainly related to crystal structure, electronic conduction is determined by the electronic bandgap.

The conductivity is proportional to the concentration of charge carriers noted c_i carriers/Volume; the charge they carry is $z_i e$ (C/charge), where e is the unit electronic charge, mobility noted μi, which is their ability to move in an electric field.

Having z_i unit charges on the carrier is described for their mobility to move in an electric field by their mobility μ_i; the conductivity is described by the relations

$$\sigma_i = c_i z_i e \mu_i \tag{11}$$

where c_i is the concentration of charge carriers per volume and $z_i e$ the charge they carry in C per charge.

In response to a concentration gradient, the system attempts to return to a homogenous equilibrium state by eliminating the gradient. The Fick's first law describes the unidirectional diffusion:

$$J_i = D_i \frac{dc_{i-}}{dx} \tag{12}$$

where dc_i/dx is the concentration gradient of species i, J_i is its flux in particles*cm^{-2}*s^{-1}, and D_i is the diffusion constant in particles*cm^{-4}.

5. Clean energy applications

5.1 Perovskites in solid oxide fuel cell

A solid oxide fuel cell, SOFC, essentially consists of two porous electrodes separated by a dense, oxide ion-conducting electrolyte. The operating principle of such a cell is illustrated in **Figure 6**. The oxygen supplied at the cathode or, air electrode, reacts with incoming electrons from the external circuit to form oxide ions, which migrate to the anode or, fuel electrode, through the oxide ion conducting electrolyte. At the anode side, the oxide ions combine with H_2, CO in the fuel to form H_2O, CO_2, with the effect of liberating electrons. Electrons flow from the anode through the external circuit to the cathode. To keep the cell resistance low, the electrolyte is fabricated in the form of a thin film.

Due to its operating conditions there are some limitations to materials used for SOFC.

These materials should be durable without changes of the required properties. Until now, there have been several researches to develop and fabricate materials to meet requirements of SOFC. **Table 1** summarizes such perovskite materials accordingly to the SOFC component.

Electrolyte may carry either oxide ion O^{2-} or proton H^+ and should have high ionic conductivity and uniform features in structure. The important properties of cathodes are high electronic conductivity and thin porous layer where the oxygen reduction reaction takes place. The anode materials must be chemically compatible with electrolyte. Thermal expansion also is a requirement to match with electrolyte thermal expansion characteristics. The thermal expansion of solids depends on their structure symmetry and may be either isotropic or anisotropic. Properties like electrical conductivity, large triple phase boundary, and high electrocatalytic

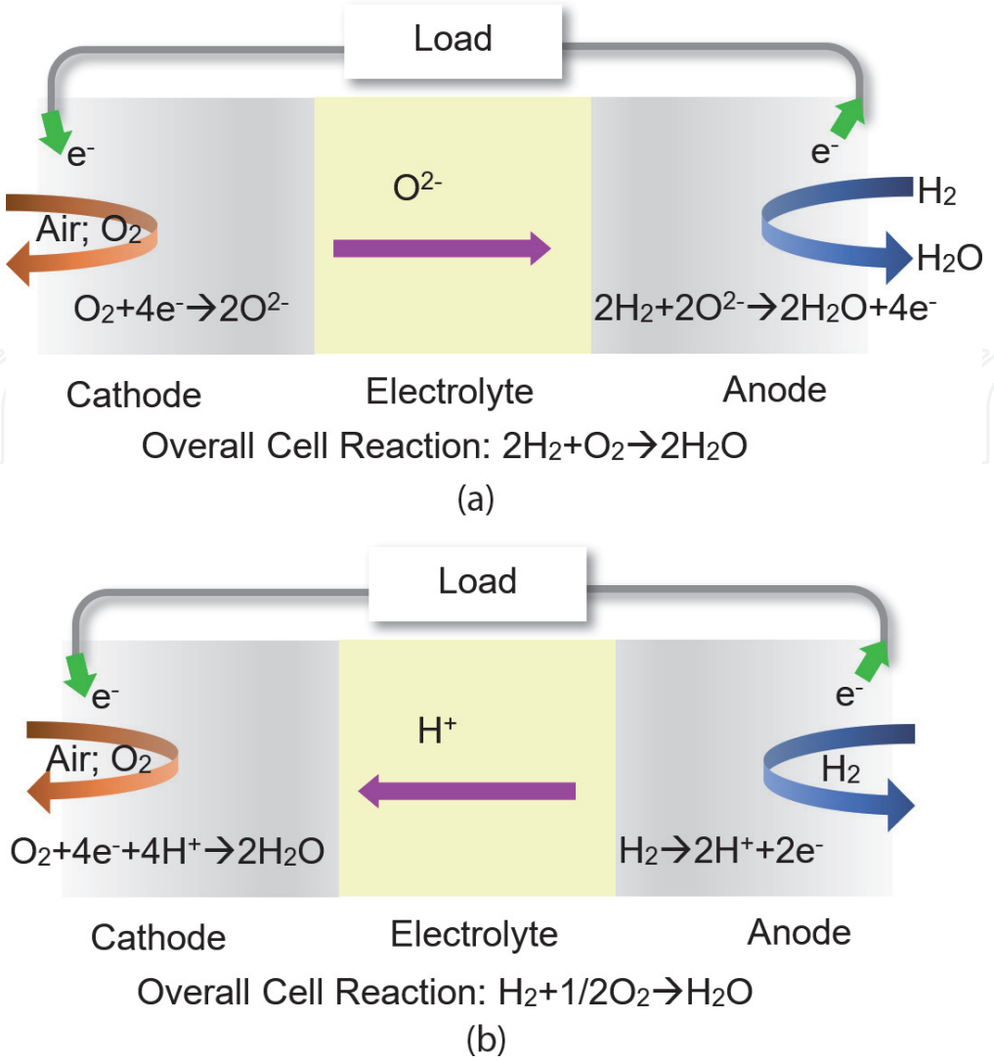

Figure 6.
Operating principle of a solid oxide fuel cell. (a) Operating principle of a solid oxide fuel cell: Oxygen ion-conducting type cell. (b) Operating principle of a solid oxide fuel cell: Hydrogen ion-conducting type cell.

Component part	Material
Electrolyte	$LaGaO_3$-type [30]: (La,Sr)(Ga,Mg)O_3, (La,Sr)(Ga,MgCo)O_3, (La,Sr)(Ga,Mg,Fe)O_3, (La,Sr)(Ga,Mg,Co,Fe)O_3 $LaAlO_3$-type [31]: (La,Ca)AlO_3, (La,Ba)AlO_3 Brownmillerite perovskite: $BaZrO_3$ [32]
Cathode	$LaMnO_3$-type [33]: (La,Sr)MnO_3, (La,Ca)MnO_3 LaCoO3-type [34]: (La,Sr)CoO_3, (La,Ca)CoO_3 (La,Sr)FeO_3 [35] (Sm,Sr)CoO_3, (Sm,Nd)CoO_3, $LaNiO_3$ K_2NiF_4 structure
Anode	$SrNbO_3$ [36]; $SrVO_3$ [37]
Separator	$LaCrO_3$ type [38, 39]: (La,Sr)CrO_3, (La,Ca)CrO_3

Table 1.
Typical materials used in solid oxide fuel cells.

activity provide a mechanism for electronic conductivity, constituting important qualities to take in account from anode materials. Among the materials developed for SOFC components, (La, Sr)MnO_3 in air shows a conductivity of 300 S/cm [40],

(La, Sr)(Co, Fe)O_3 about 330 S/cm [41], and (La, Sr)CoO_3 about 1.22–1.60 S/cm [42, 43]. (Pr, Ba, Sr)(Co, Fe)O_5 is a promising cathode material with power densities about 2.2 W/cm^2 at 600°C and has potential for commercially viable SOFC technologies [44]. The choice of material combinations for the SOFC components is crucial for determining their performances.

5.2 Perovskites in catalysis

Transition metal perovskites are important catalyst materials. The catalytic activity for perovskite materials often resides with metal oxide surface sites, and efficient use of the metals and space available requires small particles, located on a mostly inert support to enhance the thermal stability of the catalyst. Direct electrochemical water splitting is considered a key process in the development of novel energy storage systems, crucial for a sustainable and environmentally friendly energy economy. Water electrolyzers can convert water into hydrogen and oxygen through an electrochemical process, allowing H_2 to be stored as an energy vector as is seen in **Figure** 7.

However, the overpotentials at the anode side where the oxygen evolution reaction, OER, takes place are substantial, even when highly active, precious metal catalysts are used. Therefore, the development of anode materials based on inexpensive and abundant elements, displaying both high OER activity and stability, appears to be a crucial point toward the development of new-generation hydrogen-based storage systems. The values of OER activity about four times higher than that of bulk $LaCoO_3$ compound which was found to be 1.87 A/g were reported for porous and nanosphere $LaCoO_3$. For porous $LaCoO_3$, an OER activity of 7.51 A/g was reported, and for hollow $LaCoO_3$ nanospheres, an OER activity of 12.58 A/g was reported. Both values are at 1.60 V [45].

The oxygen evolution reaction OER in alkaline has the net reaction:

$$4HO^- = 2H_2O + O_2 + 4e^- \tag{13}$$

Typically in electrocatalysis the ion of interest is the B site assumed to be an active site for OER. From a crystal field theory perspective, the octahedrally coordinated B site state d will split into several levels. The states of interest for catalysis will be the antibonding e_g and t_{2g} states since they are typically the occupied states with highest energy and their filling will roughly determine the strength of the B-O bond.

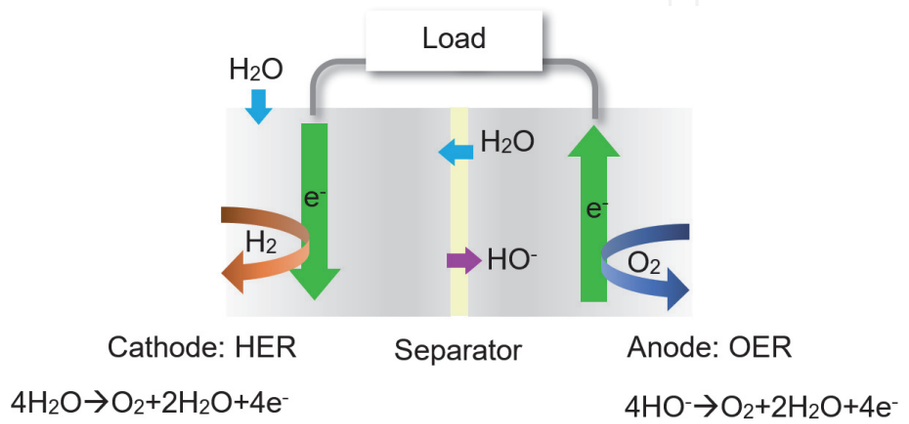

Figure 7.
Working principle of an alkaline electrolysis cell. When the direct current is applied to the water, oxygen and hydrogen are separated from the water. Oxygen arises at the anode while the hydrogen at the cathode.

The OER activities of a series of perovskites were found to form a volcano trend when plotted versus the e_g orbital filling determined using X-ray absorption near-edge structure (XANES) and spin states inferred [46]. Perovskites with an e_g orbital occupancy of approximately 1 were found to be the most active. Based on this principle, highly active perovskite catalysts like $Ba_{0.5}Sr_{0.5}Co_{0.8}Fe_{0.2}O_3$ with a conductivity of 8.58×10^{-5} S/cm, $LaNiO_3$ which has 2.39 S/cm, and $LaCoO_3$ can be used to rationally choose materials as candidates for promising OER catalyst [45, 47–52].

5.3 Perovskites in photocatalysis

In general, an efficient photocatalyst, also called an ideal semiconductor, should include light-harvesting and redox capabilities to facilitate the desired chemical reactions, thus achieving the targeted reaction. Inorganic semiconductor materials should have adequate capability to absorb solar energy across a broad spectrum. Because of their light-harvesting property, potential photocatalysts absorb solar energy, leading to the generation of photoelectrons in the conduction band and holes in the valence band for their possible use in redox reactions.

The redox nature of a photocatalyst as an intrinsic property dictates solar energy conversion efficiency. Most semiconductors include metals/mixed metal oxides used as efficient photocatalysts with the exceptional adaptability of their properties

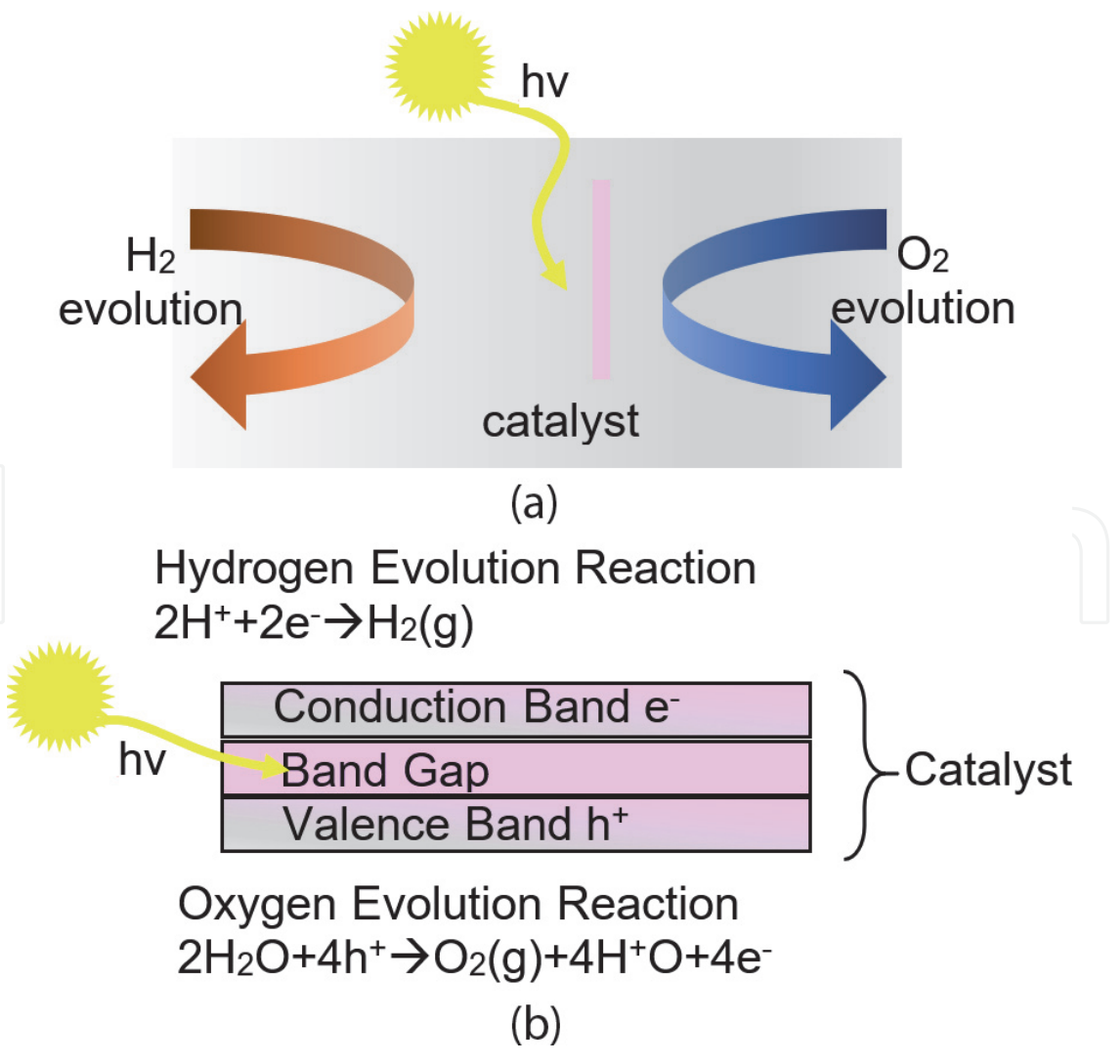

Figure 8.
Schematic of the reaction processes involved in overall water splitting. (a) The processes of photocatalytic water splitting. (b) Water molecules are oxidized by the holes to form O_2 and reduced by the electrons to form H_2.

through compositional variations; perovskites show promise for solar hydrogen production among the large number of photocatalysts being explored. As example of photocatalysts can be mentioned perovskites with formula $AFeO_3$, where A: La, Pr, Ce, and perovskites with formula $LaBO_3$ where B: Co, Mn, Fe [53–55]. Under visible light $LaFeO_3$ with a bandgap of 2.1 eV has an oxygen evolution rate of 331.5 μmol/h*g in ethanol [56]; $SrTiO_3$ with a bandgap of 3.2 eV has a rate of 18.8 μmol/h*g in ethanol [57]. Perovskite materials are also frequently explored in combination with other oxides to carry out various steps of complex uphill reactions involved in water splitting reactions. In **Figure 8**, the schematic of the reaction processes involved in overall water splitting is shown. When the energy of incident light is larger than that of a bandgap, electrons and holes are generated in the conduction and valence bands, respectively.

The perovskites tailored through bandgap engineering approaches can harvest solar light more effectively. Such perovskites show broadband absorption over the visible to near-infrared region of the solar spectrum. Another challenge related to the charge separation between photogenerated holes and electrons has also been undertaken with perovskite compositions to achieve overall improved efficiency.

6. Conclusions and outlook

In the last years environment-friendly and clean energy have attracted worldwide attention due to the growing concerns about global warming and other environmental issues associated with the heavy consumption of fossil fuels. Currently, new functional materials and adaptations to existing functional materials and their use are undergoing extensive investigation and have seen a remarkable development. Perovskites drive interest in their research investigations because the promise of their excellent features to be used in important technological devices such as the solid oxide fuel cell, water electrolysis, and photocatalysts.

We described the observed remarkable feature of adjustable structure properties for perovskites, leaving room for obtaining perovskite oxides with better functional performances. The perovskite structure is viable to wide departures in compositions from the ideal formula ABO_3. The presence of defects can change the properties of the material. When these are properly controlled, defects are the material engineer's way of tuning material properties into wanted effects.

For real world applications, there are still some challenges to tackle in order to achieve the primary goal of the energy field when perovskites with different morphologies are the target materials. Oxide perovskite materials are a competitive alternative to low-cost non-noble metal-based functional materials with high activity and stability to replace the state-of-the-art material. Approaches to prepare perovskites are usually complicated and need harsh reaction conditions like high temperatures, in most of the cases. The large-scale synthesis of perovskites is also a great challenge to researchers since most work is still limited to laboratory scale. Therefore, searching for new facile and environmentally friendly approach to synthesize perovskites is still of great importance in this field.

It can be seen from the above discussion that there are many positive outcomes in the continuous development of perovskite materials rationally engineered by defect chemistry and controlled morphologies through the preparation methods. Great efforts are dedicated for the use of *in-situ* characterization techniques like X-ray diffraction or microscopy, so we can explain how structural modifications, alterations in the morphology, degradation speed of perovskite happened. Moving toward commercialization it is necessary to ensure low cost and long-term stability of materials which represent a significant active research direction.

Acknowledgements

This work was supported by the National Authority for Scientific Research and Innovation/Romanian Ministry of Education and Research, project "RESTORE"—117/16.09.2016 ID/Cod My SMIS: P_37_595 / 104958.

Conflict of interest

The authors state that there is no conflict of interest associated with this work.

Author details

Mirela Dragan[1*], Stanica Enache[1], Mihai Varlam[1] and Konstantin Petrov[2]

1 National R&D Institute for Cryogenic and Isotope Technologies, Ramnicu Valcea, Romania

2 Academician Evgeni Budevski Institute of Electrochemistry and Energy Systems, Sofia, Bulgaria

*Address all correspondence to: mirela.dragan@icsi.ro

References

[1] Thurnaurer H, Deaderick J. U.S. Patent No. 2,429,588 filed (1941); 1947

[2] Bednorz JG, Müller KA. Possible high T superconductivity in the Ba—La—Cu—O system. Zeitschrift fur Physik B: Condensed Matter. 1986; **64**(2):189-193. DOI: 10.1007/BF01303701

[3] Tonui P, Oseni SO, Sharma G, Yan Q, Mola GT. Perovskites photovoltaic solar cells: An overview of current status. Renewable and Sustainable Energy Reviews. 2018;**91**: 1025-1044. DOI: 10.1016/j.rser.2018.04.069

[4] Alvarez G, Conde-Gallardo A, Montiel H, Zamorano R. About room temperature ferromagnetic behavior in $BaTiO_3$ perovskite. Journal of Magnetism and Magnetic Materials. 2016;**401**:196-199. DOI: 10.1016/j.jmmm.2015.10.031

[5] Zheng T, Wu J, Xiao D, Zhu J. Recent development in lead-free perovskite piezoelectric bulk materials. Progress in Materials Science. 2018;**98**:552-624. DOI: 10.1016/j.pmatsci.2018.06.002

[6] Li X, Jeanloz R. Electrical conductivity of $(Mg,Fe)SiO_3$ perovskite and a perovskite-dominated assemblage at lower. Geophysical Research Letters. 1987;**14**(11):1075-1078. DOI: 10.1029/GL014i011p01075

[7] Presto S, Kumar P, Varma S, Viviani M, Singh P. Electrical conductivity of NiMo-based double perovskites under SOFC anodic conditions. International Journal of Hydrogen Energy. 2018;**43**(9): 4528-4533. DOI: 10.1016/j.ijhydene.2018.01.066

[8] Rubel MHK, Miura A, Takei T, Kumada N, Mozahar Ali N, Nagao M, et al. Superconducting double perovskite bismuth oxide prepared by a low-temperature hydrothermal reaction. Angewandte Chemie International. 2014;**53**(14):3599-3603. DOI: 10.1002/ANIE.201400607

[9] Kim DC, Baranov AN, Kim JS, Kang HR, Kim BJ, Kim YC, et al. High pressure synthesis and superconductivity of $Ba_{1-x}K_xBiO_3$ ($0.35<x<1$). Physica C: Superconductivity. 2003;**383**(4):343-353. DOI: 10.1016/S0921-4534(02)01332-1

[10] Phraewphiphat T, Iqbal M, Suzuki K, Matsuda Y, Yonemura M, Hirayama M, et al. Syntheses, structures, and ionic conductivities of perovskite-structured lithium–strontium–aluminum/gallium–tantalum-oxides. Journal of Solid State Chemistry. 2015;**225**:431-437. DOI: 10.1016/j.jssc.2015.01.007

[11] Salles C, Bassat JM, Fouletier J, Marinha D, Steil M-C. Oxygen pressure dependence of the ionic conductivity of iron-doped calcium titanate. Solid State Ionics. 2018;**324**:103-108. DOI: 10.1016/j.ssi.2018.06.014

[12] Lin Q, Yang X, Lin J, Guo Z, He Y. The structure and magnetic properties of magnesium-substituted $LaFeO_3$ perovskite negative electrode material by citrate sol-gel. International Journal of Hydrogen Energy. 2018;**43**(28): 12720-12729. DOI: 10.1016/j.ijhydene.2018.03.156

[13] Goswami S, Bhattacharya D. Magnetic transition at ~150 K in nanoscale $BiFeO_3$. Journal of Alloys and Compounds. 2018;**738**:277-282. DOI: 10.1016/j.jallcom.2017.12.107

[14] Zhang F, Zhang X, Jiang G, Li N, Hao Z, Qu S. H_2S selective catalytic oxidation over Ce substituted. Chemical Engineering Journal. 2018;**348**:831-839. DOI: 10.1016/j.cej.2018.05.050

[15] Wang WL, Meng Q, Xue Y, Weng X, Sun P, Wu Z. Lanthanide perovskite catalysts for oxidation of chloroaromatics: Secondary pollution and modifications. Journal of Catalysis. 2018;**366**:213-222. DOI: 10.1016/j.jcat.2018.07.022

[16] Fang M, Yao X, Li W, Li Y, Shui M, Shu J. The investigation of lithium doping perovskite oxide $LiMnO_3$ as possible LIB anode material. Ceramics International. 2018;**44**(7):8223-8231. DOI: 10.1016/j.ceramint.2018.02.002

[17] Yao C, Zhang H, Liu X, Meng J, Zhang X, Meng F, et al. Characterization of layered double perovskite $LaBa_{0.5}Sr_{0.25}Ca_{0.25}Co_2O_{5+\delta}$ as cathode material for intermediate-temperature solid oxide fuel cells. Journal of Solid State Chemistry. 2018;**265**:72-78. DOI: 10.1016/j.jssc.2018.05.028

[18] Parganiha Y, Kaur J, Dubey V, Shrivastavac R. $YAlO_3:Ce^{3+}$ powders: Synthesis, characterization, thermoluminescence and optical studies. Superlattices and Microstructures. 2015;**85**:410-417. DOI: 10.1016/j.spmi.2015.06.011

[19] Baig HN, Saluja JK, Haranath D. Investigation of luminescence properties of Dy^{3+} doped $YAlO_3$ phosphors synthesized through solid state method. Optik. 2016;**127**(20): 9178-9195. DOI: 10.1016/j.ijleo.2015.12.159

[20] Zhang Y, Tso CY, Iñigo JS, Liu S, Miyazaki H, Chao CYH, et al. Perovskite thermochromic smart window: Advanced optical properties and low transition temperature. Applied Energy. 2019;**254**:113690. DOI: 10.1016/j.apenergy.2019.113690

[21] Matsouka C, Zaspalis V, Nalbandian L. Perovskites as oxygen carriers in chemical looping reforming process—Preparation of dense perovskite membranes and ionic conductivity measurement. Materials Today: Proceedings. 2018;**5**(14): 27543-27552. DOI: 10.1016/j.matpr.2018.09.074

[22] Baek D, Kamegawa A, Takamura H. Mixed conductivity and electrode properties of Mn-doped Bi–Sr–Fe-based perovskite-type oxides. Solid State Ionics. 2013;**253**:211-216. DOI: 10.1016/j.ssi.2013.09.056

[23] Swierczek K, Zajac W, Klimkowicz A, Zheng K, Malikova N, Dabrowski B. Crystal structure and proton conductivity in highly oxygen-deficient $Ba_{1-x}La_x(In, Zr, Sn)O_{3-\delta}$ perovskites. Solid State Ionics. 2015;**275**: 58-61. DOI: 10.1016/j.ssi.2015.02.018

[24] Zang M, Zhao C, Wang Y, Chen S. A review of recent advances in catalytic combustion of VOCs on perovskite-type catalysts. Journal of Saudi Chemical Society. 2019;**23**(6):645-654. DOI: 10.1016/j.jscs.2019.01.004

[25] De Graef M, McHenry ME. Structure of materials: An introduction to crystallography, diffraction and symmetry. Cambridge, United Kingdom: Cambridge University Press; 2007. p. 671. ISBN: 978-0-521-65151-6

[26] Ali R, Yashima M. Space group and crystal structure of the perovskite $CaTiO_3$ from 296 to 1720 K. Journal of Solid State Chemistry. 2005;**178**(9): 2867-2872. DOI: 10.1016/j.jssc.2005.06.027

[27] Goldschmidt VM. Die gesetze der krystallochemie. Die Naturwissenschaften. 1926;**21**:477-485. DOI: 10.1007/bf01507527

[28] Dragan M, Misture S. In-situ analysis of chemical expansion and stability of SOFC cathodes. Materials Research Society Symposium Proceedings. 2014;**1655**:77-82. DOI: 10.1557/opl.2014.413

[29] Knyazev AV, Mączka M, Krasheninnikova OV, Ptak M, Syrov EV, Trzebiatowska-Gussowska M. High-temperature X-ray diffraction and spectroscopic studies of some Aurivillius phases. Materials Chemistry and Physics. 2018;**204**:8-17. DOI: 10.1016/j.matchemphys.2017.10.022

[30] Zhu C, Nobuta A, Ju YW, Ishihara T, Akiyama T. Solution combustion synthesis of $Ce_{0.6}Mn_{0.3}Fe_{0.1}O_2$ for anode of SOFC using $LaGaO_3$-based oxide electrolyte. International Journal of Hydrogen Energy. 2013;**38**(30):13419-13426. DOI: 10.1016/j.ijhydene.2013.08.007

[31] Fu QX, Tietz F, Lersch P, Stover D. Evaluation of Sr- and Mn-substituted $LaAlO_3$ as potential SOFC anode materials. Solid State Ionics. 2006;**177**(11–12):1059-1069. DOI: 10.1016/j.ssi.2006.02.053

[32] Xie H, Wei Z, Yang Y, Chen H, Ou X, Lin B, et al. New Gd-Zn co-doping enhanced mechanical properties of $BaZrO_3$ proton conductors with high conductivity for IT-SOFCs. Materials Science and Engineering B. 2018;**238–239**:76-82. DOI: 10.1016/j.mseb.2018.12.012

[33] Shimada H, Yamaguchi T, Sumi H, Nomura K, Yamaguchi Y, Fujishiro Y. Extremely fine structured cathode for solid oxide fuel cells using Sr-doped $LaMnO_3$ and Y_2O_3-stabilized ZrO_2 nano-composite powder synthesized by spray pyrolysis. Journal of Power Sources. 2017;**341**:280-284. DOI: 10.1016/j.jpowsour.2016.12.002

[34] Dragan M, Enache S, Varlam M, Petrov K. Perovskite-type material lanthanum cobaltite $LaCoO_3$: aspects of processing route toward practical applications. In: Cobalt Compounds and Applications. Rijeka, Croatia: IntechOpen Limited; 2019. DOI: 10.5772/intechopen.86260. ISBN: 978-1-78984-559-4

[35] Lakshminarayanan N, Kuhn JN, Rykov SA, Millet JMM, Ozkan US. Doped $LaFeO_3$ as SOFC catalysts: Control of oxygen mobility and oxidation activity. Catalysis Today. 2010;**157**(1–4):446-450. DOI: 10.1016/j.cattod.2010.03.037

[36] Miruszewski T, Kamecki B, Lapinski M, Karczewski J. Fabrication, structural and electrical properties of Sr$(V,Nb)O_{3-\delta}$ perovskite materials. Materials Chemistry and Physics. 2018;**212**:446-452. DOI: 10.1016/j.matchemphys.2018.03.070

[37] Yaremchenko AA, Brinkmann B, Janssen R, Frade JR. Electrical conductivity, thermal expansion and stability of Y- and Al-substituted $SrVO_3$ as prospective SOFC anode material. Solid State Ionics. 2013;**247–248**:86-93. DOI: 10.1016/j.ssi.2013.06.002

[38] Jiang SP, Liu L, Ong KP, Wu P, Li J, Pu J. Electrical conductivity and performance of doped $LaCrO_3$ perovskite oxides for solid oxide fuel cells. Journal of Power Sources. 2008;**176**(1):82-89. DOI: 10.1016/j.jpowsour.2007.10.053

[39] Guo P, Zeng C, Shao Y. Effect of $LaCrO_3$ coating on high temperature oxidation of type 316 stainless steel. Journal of Rare Earths. 2011;**29**(7):698-701. DOI: 10.1016/S1002-0721(10)60525-X

[40] Trasatti S. Water electrolysis: Who first? Journal of Electroanalytical Chemistry. 1999;**476**(1):90-91. DOI: 10.1016/S0022-0728(99)00364-2

[41] Enache S, Dragan M, Varlam M, Petrov K. Electronic percolation threshold of self-standing Ag-$LaCoO_3$ porous electrodes for practical applications. Materials. 2019;**12**(15):2359. DOI: 10.3390/ma12152359

[42] Enache S, Dragan M, Soare A, Petrov K, Varlam M. Environmentally

friendly methods for high quality lanthanum cobaltite perovskite catalyst synthesis. Progress of Cryogenics and Isotopes Separation. 2019;**22**(1):39

[43] Enache S, Dragan M, Soare A, Ebrasu DI, Zaulet A, Varlam M, et al. One step solid-state synthesis of lanthanum cobalt oxide perovskites as catalysts for oxygen evolution in alkaline media. Bulgarian Chemical Communications. 2018;**50**(A):127-132

[44] Jiang SP. A comparison of O_2 reduction reactions on porous (La,Sr) MnO_3 and (La,Sr)(Co,Fe)O_3 electrodes. Solid State Ionics. 2002;**146**(1–2):1-22. DOI: 10.1016/S0167-2738(01)00997-3

[45] Manwar NR, Borkar RG, Khobragade R, Rayalu SS, Jain SL, Bansiwal AK, et al. Efficient solar photo-electrochemical hydrogen generation using nanocrystalline $CeFeO_3$ synthesized by a modified microwave assisted method. International Journal of Hydrogen Energy. 2017;**42**(16): 10931-10942. DOI: 10.1016/j.ijhydene.2017.01.227

[46] Petric A, Huang P, Tietz F. Evaluation of La–Sr–Co–Fe–O perovskites for solid oxide fuel cells and gas separation membranes. Solid State Ionics. 2002;**135**(1–4):719-725. DOI: 10.1016/S0167-2738(00)00394-5

[47] Tietz F, Arul Raj I, Zahid M, Mai A, Stover D. Survey of the quasi-ternary system $La_{0.8}Sr_{0.2}MnO_3$–$La_{0.8}Sr_{0.2}CoO_3$–$La_{0.8}Sr_{0.2}FeO_3$. Progress in Solid State Chemistry. 2007;**35**(2–4):539-543. DOI: 10.1016/j.progsolidstchem.2007.01.028

[48] Ullmann H, Trofimenko N, Tietz F, Stover D, Ahmad-Khanlou A. Correlation between thermal expansion and oxide ion transport in mixed conducting perovskite-type oxides for SOFC cathodes. Solid State Ionics. 2000; **138**(1–2):79-90. DOI: 10.1016/S0167-2738(00)00770-0

[49] Choi S, Yoo S, Kim J, Park S, Jun A, Sengodan S, et al. Highly efficient and robust cathode materials for low-temperature solid oxide fuel cells: $PrBa_{0.5}Sr_{0.5}Co_{2-x}Fe_xO_5$. Scientific Reports. 2013;**3**:2426. DOI: 10.1038/srep02426

[50] Dragan M, Enache S, Soare A, Petrov K, Varlam M. $LaCoO_3$ perovskite-type oxide: Synthesis and characterization towards practical applications. Progress of Cryogenics and Isotopes Separation. 2018;**21**(2):49-56

[51] Ebrasu DI, Zaulet A, Enache S, Dragan M, Carcadea E, Varlam M, et al. Electrochemical characterization of metal oxide as catalysts oxygen evolution in alkaline media. Bulgarian Chemical Communications. 2018;**50**(A): 133-138

[52] Humayun M, Sun N, Raziq F, Zhang X, Yan R, Li Z, et al. Synthesis of ZnO/Bi-doped porous $LaFeO_3$ nanocomposites as highly efficient nano-photocatalysts dependent on the enhanced utilization of visible-light-excited electrons. Applied Catalysis B: Environmental. 2018;**231**:23-33. DOI: 10.1016/j.apcatb.2018.02.060

[53] Ibarra-Rodriguez LI, Huerta-Flores AM, Mora-Hernandez JM, Torres-Martínez LM. Photocatalytic evolution of H_2 over visible-light active $LaMO_3$ (M: Co, Mn, Fe) perovskite materials: Roles of oxygenated species in catalytic performance. Journal of Physics and Chemistry of Solids. 2020;**136**:109189. DOI: 10.1016/j.jpcs.2019.109189

[54] Egelund S, Caspersen M, Nikiforov A, Moller P. Manufacturing of a $LaNiO_3$ composite electrode for oxygen evolution in commercial alkaline water electrolysis. International Journal of Hydrogen Energy. 2016;**41**(24): 10152-10160. DOI: 10.1016/j.ijhydene.2016.05.013

[55] Kim J, Chen X, Shih PC, Yang H. Porous perovskite-type lanthanum cobaltite as electrocatalysts toward oxygen evolution reaction. ACS Sustainable Chemistry & Engineering. 2017;**5**(11):10910-10917. DOI: 10.1021/acssuschemeng.7b02815

[56] Tijare SN, Joshi MV, Padole PS, Mangrulkar PA, Rayalu SS, Labhsetwar NK. Photocatalytic hydrogen generation through water splitting on nano-crystalline $LaFeO_3$ perovskite. International Journal of Hydrogen Energy. 2012;**37**(13): 10451-10456. DOI: 10.1016/j.ijhydene.2012.01.120

[57] Puangpetch T, Sreethawong T, Yoshikawa S, Chavadej S. Hydrogen production from photocatalytic water splitting over mesoporous-assembled $SrTiO_3$ nanocrystal-based photocatalysts. Journal of Molecular Catalysis A: Chemical. 2009;**312**(1–2): 97-106. DOI: j.molcata.2009.07.012